Mapping Global Star Formation in the Interacting Galaxy Pair Arp32

I. Damjanov, D. Fadda, F. Marleau, P. Appleton, P. Choi, M. Lacy, L. Storrie-Lombardi and L. Yan

Spitzer Science Center, California Institute of Technology, MC 220-6, Pasadena, CA 91125

Abstract. A multi-wavelength set of photometric data including UV (GALEX), optical, near-IR, infrared (*Spitzer*) and radio (VLA 20cm) images and spectroscopic observations are used to map the dust-obscured and unobscured star formation in the galaxy pair Arp 32. The system consists of an actively star-forming galaxy and another one with depressed star formation. The most active galaxy has disrupted morphology and different sites of star formation. Spectroscopic data show hints of nuclear activity in its core, intense star formation in limited regions of the galaxy as well as an underlying population of stars witnessing a past episode of star formation. Current star formation rates are estimated from UV and bolometric IR luminosities.

1. Introduction

The Arp 32 object ($z = 0.004$, distance ≈ 17.2 Mpc) consists of two interacting galaxies separated by $40''$ (≈ 3.3 Kpc). The system lies in the field observed with *Spitzer*, VLA, SDSS and GALEX known as First-Look Survey (see, e.g., Fadda et al. 2004). Further ancillary data were obtained with the Palomar 200" telescope: J and Ks images with WIRC and long-slit spectra with Double-spec. Finally, a *Spitzer* observation at 16 μm, taken with the IRS blue peak-up array for calibration purposes, was used. Our extended photometric dataset (UV at 1528 Å and 2271 Å, u',g',r',i',z', J, Ks, 3.6, 4.5, 5.8 and 8.0 μm IRAC, 16 μm IRS, 24, 70 and 160 μm MIPS and 20 cm VLA) allows us to map the star formation in the system with different techniques. A detailed R image (KPNO-4m, Fadda et al. 2004, Fig. 1) was used to identify the knots of infrared emission and to program the spectroscopic observations. The object was observed at three different position angles: P.A. = 14° (slit A), P.A. = 88.5° (slit B) and P.A. = 4° (slit C), with a $2''$ slit to get spectra of all the emission knots visible in the R-band image (Fig. 1). We reduced the spectra with the IRAF packages *twodspec* and *ccdred* and extracted apertures corresponding to each knot of emission. The spectra cover the range 3000-8000 Å with dispersions 1.07 Å pixel^{-1} and 2.45 Å pixel^{-1} for the blue and the red arm, respectively.

2. Spectroscopy

We measured emission and absorption line fluxes simultaneously using an IDL code to obtain emission line fluxes corrected for the underlying stellar absorption.
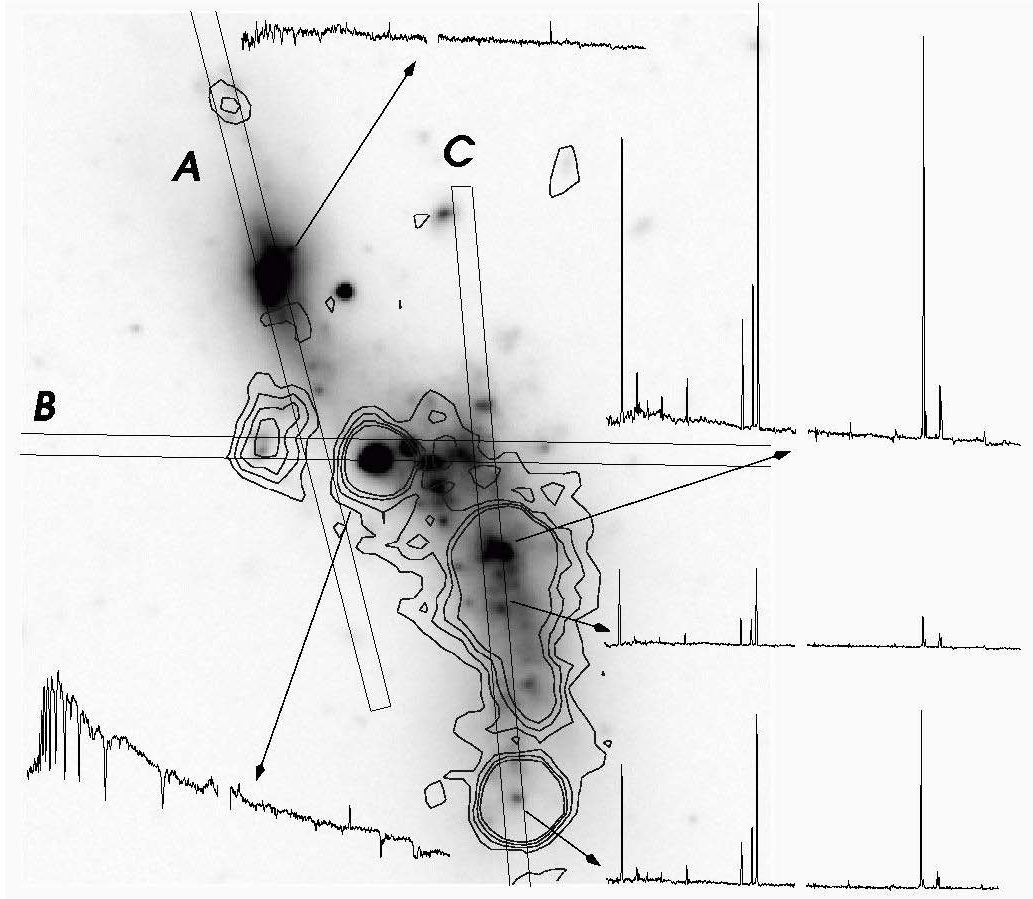
Figure 1. Arp 32 R-band image with 24 μm contours and positions of the long slits superimposed; extracted spectra for some of the emission knots are also presented. The spectrum of the nucleus of the upper galaxy shows almost no activity, while the emission lines are prominent in the nuclear part of the lower companion. Absorption features are visible in the central part of the object, in the slit B.

This mainly affects Balmer lines of the lower companion and, if uncorrected, can lead to big errors in the evaluation of reddening and star formation densities. All line fluxes were measured using multi-Gaussian profile fitting. That enabled us to deblend the Hα-[N II]$\lambda\lambda$6548,6563 triplet and the [S II]$\lambda\lambda$6716,6731 doublet, which are present in all the extracted spectra. In order to ensure reliable flux measurements, we considered only absorption and emission lines with signal-to-noise ratios (SNR) greater than 3.

Measured fluxes of the emission lines were corrected for dust reddening (i.e., internal extinction) based on the Hα/Hβ flux ratio (Calzetti 2001). When Hβ fluxes could not be reliably measured, we estimated 3-σ upper limits from the continuum SNR at $\lambda \sim 4800$ Å assuming a width similar to that of Hβ in other spectra of the same slit.
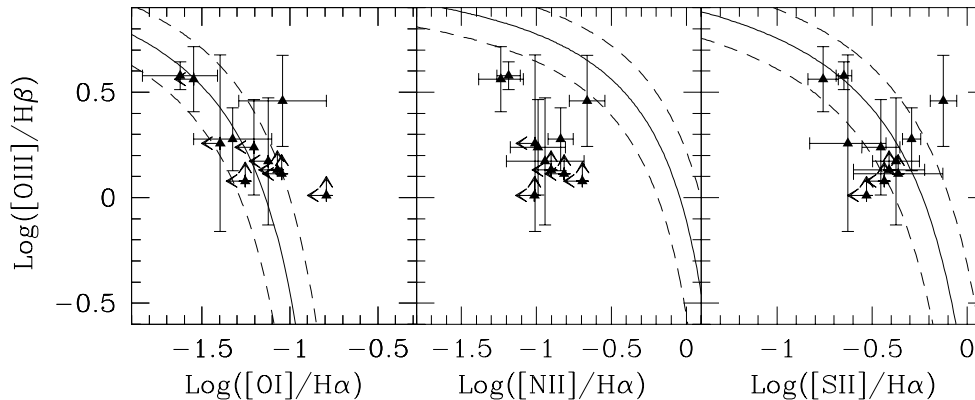
Figure 2.   VO diagnostics diagrams for the slit C; overplotted curves were taken from Kewley et al. (2001); the section below the curves in each diagram corresponds to the area occupied by the H II-like regions, while the section above the curves denotes AGN- and LINERs-like features.

The measured $H\alpha/H\beta$ ratio results in negative values for the broad-band color excess, $E(B-V)$, in some of the infrared knots. Most of these values are only lower limits since $H\beta$ fluxes could not be reliably measured, but in the nucleus of the lower companion both lines were detected with high SNR values obtaining a negative $E(B-V)$ value. Whenever reddening coefficients were determined to be negative, we assumed the Galactic interstellar extinction to compute reddening-corrected line flux densities ($E(B-V) = 0.02$). Corrected line flux densities were used to build Veilleux-Osterbrock (VO) diagnostic diagrams [O III] $\lambda5007/H\beta$ versus [O I] $\lambda6300/H\alpha$, [NII] $\lambda6583/H\alpha$ and [S II]$\lambda\lambda(6716+6731)/H\alpha$ (Kewley et al. 2001), in order to study the nature of ionizing sources in emission-line regions. All emission knots lie in the area of the diagrams occupied by the H II-like regions, except for the nucleus of the lower companion which shows AGN-like features (Fig. 2). Line flux densities were also used to estimate the metallicity of the emission knots, following the algorithm given in Kewley & Dopita (2002). The fact that the nuclear part of the lower galaxy is metal-poor ($\log(O/H)+12 < 8.5$) could possibly explain the negative values of the broad-band color excess $E(B-V)$ (e.g., Gronwall et al. 2004). Deep Balmer absorption lines are detected in the upper region of the lower galaxy (see Fig. 1) which witness a past episode of star formation.

3.   Photometry

Aperture photometry was used to measure the fluxes in all the available passbands for both galaxies. We corrected the obtained fluxes for Galactic extinction and use them to build galaxies' spectral energy distributions (SED) presented in Figure 3 . In order to compute star formation rates (SFR) based on IR luminosities, we fitted infrared SEDs with Chary & Elbaz (2001) templates. The UV, optical and near-IR part were fitted with the PEGASE (Fioc & Rocca-Volmerange
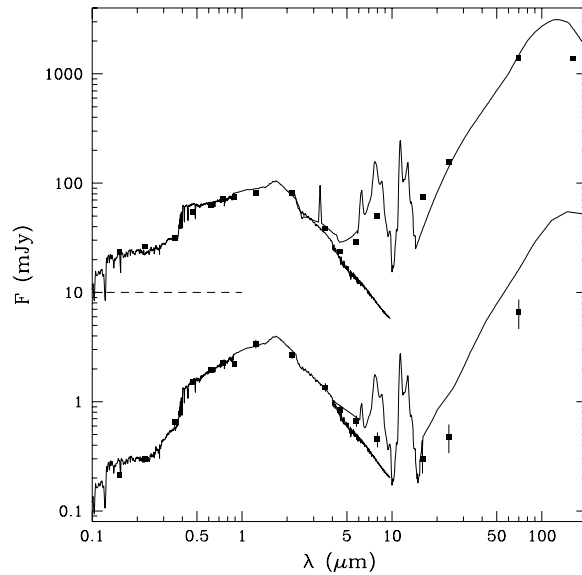
Figure 3.   SEDs for the two interacting galaxies: the bottom one corresponds to the upper companion and the top one to the lower companion. Its flux scale is shifted for presentation purposes and a dashed line denotes the zero point.

1997) models. The best fitted model for the upper galaxy corresponds to an elliptical galaxy with older stellar population (5 Gyr) and additional 10-30% of stars younger than 1 Gyr, while the lower galaxy is best fitted with SO galaxy templates with a young (0.5 -1 Gyr) stellar population. Following the equations given in Kennicutt (1998), we used the measured far-UV and IR fluxes to estimate the SFRs in both galaxies. The upper companion seems less active with a SFR value of 0.028 $M_\odot$ yr^{-1} according to its FUV flux and 0.046 $M_\odot$ yr^{-1} based on the integrated 8-1000 μm flux from the Chary & Elbaz (2001) best-fit template. The latter value is overestimated since no template fits well the data. SFR values for the lower galaxy are 0.12 $M_\odot$ yr^{-1} and 1 $M_\odot$ yr^{-1} based on FUV flux and integrated IR flux, respectively, showing therefore a large amount of obscured star formation.

References

Calzetti, C. 2001, PASP, 113, 1449
Chary, R., & Elbaz, D. 2001, A&A, 556, 562
Fadda, D., Jannuzi, B. T., Ford, A., Storrie-Lombardi, L. J., 2004, AJ, 128, 1
Fioc, M., & Rocca-Volmerange, B. 1997, A&A, 326, 950
Gronwall, C., Jangren, A., Salzer, J. J., et al., 2004, ApJ, 128, 644
Kennicutt, R. 1998, ARA&A, 36, 189
Kewley, L. J., Dopita, M. A., Sutherland, R. S., et al., 2001, ApJ, 556, 121
Kewley, L. J., & Dopita, M. A. 2002, ApJS, 142, 35